JAST, Vol. 4, No. 1, pp 39–47

JAST
Journal of Aerospace Science and Technology

Numerical Investigation of Rotating-Stall in a Stage of an Axial Compressor with Two Different Approaches

N. Amanifard[1], B. Farhanieh[2], K. Ghorbanian[3]

Rotating-Stall (RS) through a cascade of an axial compressor has been numerically investigated by employing an unsteady two-dimensional finite-volume density based computer code. To validate the computer code, three test cases were prepared, and the good agreement resulting from comparison of the results has given adequate assurance of the code. The cascade problem was studied through different geometric approaches, which were classified in two main categories. The first was the semi-stage (single rotor-cascade), and the second was the complete stage. For each geometric approach, the number of blades was varied from a minimum number to a maximum value (variable cascade length). The RS modal characteristics and its development for all geometric cases were observed. The RS was incepted with a 40% reduction in flow coefficient and a 0.4% increase in the load coefficient from their normal operating values. In all cases, the captured modal characteristics of RS varies with the variation of the cascade length to a maximum value, and this triggers the same modes of RS. The variation of the modal characteristics of the RS, in the two main geometric approaches seems to be similar, but at different levels.

INTRODUCTION

Analysis of the flow field in unstable condition, especially in Gas-Turbine engines, has been mainly based on experimental observations and studies for the last decade [1-3]. Recently, several computational fluid dynamics (CFD) codes have been developed. From the viewpoint of flow instability phenomena, axial compressors with their adverse pressure gradients in through flow direction are the most critical component in Gas-Turbine engines. Today, using CFD tools is a standard practice in the study of cascade flow within the stable operating range of a compressor, but the CFD approach still needs to be established as a sound prediction method for operation in the unstable region. Notable progress in the use of CFD-type techniques for calculation of instability effects has been made by Sisto *et.al.* [4] and Jonnavithula *et.al.* [5]. They used a two-dimensional discrete vortex model, with the separation point being obtained by an integral boundary layer. The evolution of stall is well predicted in their experiment, although only up to six blade passages are used in the computation. Further, a numerical study was made by He [6] in a single stage axial compressor. The Navier-Stokes equations were discretized in space by finite volume method, and integrated in time by a four stage Rung-Kutta scheme. The second- and fourth-order blended smoothing was adopted in both the stream wise and circumferential directions for numerical damping. Baldwin-Lomax turbulence model was also adopted. Outa *et.al.* [7] made a numerical simulation for stall cells in rotor-stator frame of a compressor using viscous approach. Furthermore, a numerical study was done by Saxer *et.al.* [8] on inviscid flow passing through axial compressors, and the history of stall vortices were investigated for a fifteen-blade passage of a single stage. The mass flow rate fluctuations were approximately similar to those obtained from their experimental observations.

In previous CFD works on RS, one can not find

1. *Assistant Professor, Dept. of Mech. Eng., Guilan Univ., Rasht, Iran, Email: namanif@guilan.ac.ir.*
2. *Professor, Dept. of Mech. Eng., Sharif Univ. of Tech., Tehran, Iran.*
3. *Associate Professor, Dept. of Aerospace Eng., Sharif Univ. of Tech., Tehran, Iran.*

any criterion for choosing the number of blades and the geometric approaches. The scope of this work is to propose an adequate number of blades in CFD studies of RS, and to compare the effect of using a free-rotor cascade in place of a complete stage on RS modal shapes.

GOVERNING EQUATIONS

In Cartesian coordinate, let $\mathbf{Q}$ be an unknown vector defined for a two-dimensional study as follows:

$$\mathbf{Q} = [\rho, \rho u, \rho v, \rho E]^T = [q_1, q_2, q_3, q_4]^T, \quad (1)$$

where E is the total energy ($E = e + (u^2 + v^2)/2$), ρ is the density, u is the axial velocity component and v is the tangential velocity component. Let V be any volume with bounding surface ∂V and outward unit normal $\mathbf{n}$. Assuming that the volume does not vary with time, $\mathbf{Q}$ satisfies the following integral conservation law:

$$\frac{d}{dt}\int_V \mathbf{Q}dV = \int_V \frac{\partial}{\partial t}\mathbf{Q}dV = -\oint_{\partial V} \hat{\mathbf{E}}.\mathbf{n}dS. \quad (2)$$

The equivalent differential form of Equation (2) in an inertial reference system reads:

$$\frac{\partial}{\partial t}\mathbf{Q} = -\nabla.\hat{\mathbf{E}}. \quad (3)$$

This accounts for the inviscid ($\hat{\mathbf{E}}_E$) and viscous ($\hat{\mathbf{E}}_V$) contributions, *i.e.*

$$\hat{\mathbf{E}} = \hat{\mathbf{E}}_E - \hat{\mathbf{E}}_V, \quad (4)$$

where

$$\hat{\mathbf{E}}_E = [\rho\mathbf{u}, \rho\mathbf{u}\mathbf{u} + p\mathbf{I}, \rho\mathbf{u}(E + P/\rho)]^T, \quad (5a)$$

$$\hat{\mathbf{E}}_V = [0, \sigma, -(\mathbf{q} - \mathbf{u}.\sigma)]^T, \quad (5b)$$

and

$$\sigma = \mu\left(\nabla\mathbf{u} + \nabla\mathbf{u}^{\mathbf{T}}\right) - \frac{2}{3}\mu\nabla.\mathbf{u}\mathbf{I}, \quad (6)$$

$$\mathbf{q} = -\lambda\nabla T. \quad (7)$$

The governing equations are transformed to a computaional space for the numerical solution. Hence, they are as follows:

$$\frac{\partial\overline{\mathbf{Q}}}{\partial\tau} + \frac{\partial\overline{\mathbf{E}_E}}{\partial\xi} + \frac{\partial\overline{\mathbf{F}_E}}{\partial\eta} = \frac{\partial\overline{\mathbf{E}}_v}{\partial\xi} + \frac{\partial\overline{\mathbf{F}}_v}{\partial\eta}, \quad (8)$$

$\overline{\mathbf{Q}}$ is the premitive variables matrix, $\overline{\mathbf{E}}_E$ and $\overline{\mathbf{F}}_E$ are the transformed convective flux matricies in ζ and η directions respectively, and $\overline{\mathbf{E}}_\nu$ and $\overline{\mathbf{F}}_\nu$ are the transformed viscous matrices in ζ and η directions in turn. τ is the dimensionless time variable, $\mathbf{u}$ is the velocity vector, $\mathbf{q}$ is the heat flux, $\mathbf{I}$ is the identity matrix, μ is the absolute viscosity and λ is the thermal conductivity. The superscript T denotes the transpose matrix assignment.

Regarding the two-dimensional approach in present work, the governing equations for relative frame are the same as those in the absolute frame because there is no Coriolis acceleration (no radial component of velocity). Additionally, the stagnation enthalpy is constant in the relative frame and as a result there is no energy transfer between the fluid and the blades in the relative coordinate. Consequently, the only treatment in stationary-cascade studies (if desired) is the using of absolute velocities in place of relative velocities in the solver. As evident, the absolute velocities are achieved by adding the rotation speed to relative velocities.

NUMERICAL PROCEDURE

Finite-Volume Formulation

Reconsidering Equation (8), the time derivative is approximated by a first-order backward differencing quotient and the remaining terms are evaluated at time level $n + 1$. Thus:

$$\frac{\overline{\mathbf{Q}}^{n+1} - \overline{\mathbf{Q}}^n}{\Delta\tau} + (\frac{\partial\overline{\mathbf{E}}}{\partial\xi})^{n+1} + (\frac{\partial\overline{\mathbf{F}}}{\partial\eta})^{n+1} = (\frac{\partial\overline{\mathbf{E}_v}}{\partial\xi})^{n+1} + (\frac{\partial\overline{\mathbf{F}_v}}{\partial\eta})^{n+1}. \quad (9)$$

Integrating Equation (9) over square **ABCD** shown in Figure 1, and using Green's theorem provides:

$$\Delta\overline{\mathbf{Q}} + \frac{\Delta\tau}{\Delta\xi}(\overline{\mathbf{E}}_{Er} - \overline{\mathbf{E}}_{El}) + \frac{\Delta\tau}{\Delta\eta}(\overline{\mathbf{F}}_{Et} - \overline{\mathbf{F}}_{Eb}) = \frac{\Delta\tau}{\Delta\xi}(\overline{\mathbf{E}}_{vr} - \overline{\mathbf{E}}_{vl}) + \frac{\Delta\tau}{\Delta\eta}(\overline{\mathbf{F}}_{vt} - \overline{\mathbf{F}}_{vb}), \quad (10)$$

Since, in Equation (10), the flux vectors are evaluated in time step $n + 1$; they can be expressed in terms of $\Delta\overline{\mathbf{Q}}$, by using the Taylor expansion and a first order approximation in time.([9])

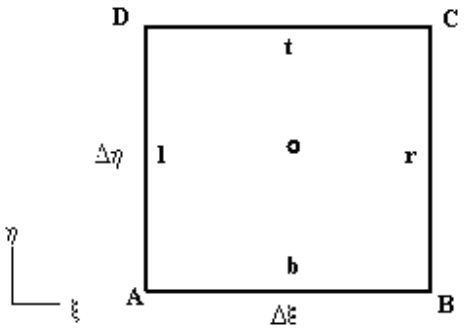

Figure 1. The Finite Volume Cell.

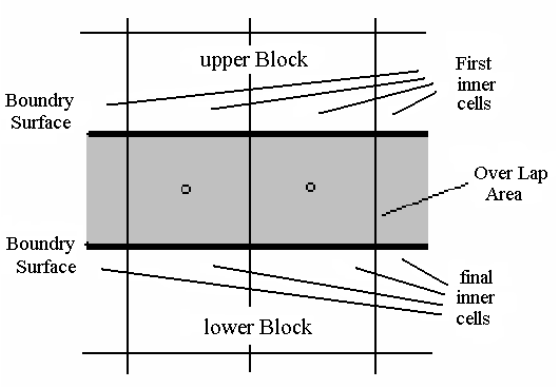

Figure 2. Schematic shape of Block Boundary Condition.

The inviscid flux vectors on cell faces were evaluated by Van-Leer's Flux splitting scheme. To prevent the oscillatory behavior of the numerical results and to increase the accuracy, the Van-Leer's limiter was added to the flux splitting algorithm ([10]).

The second-order derivatives are evaluated by central difference approximation.

Numerical Boundary Conditions

Regarding the subsonic inflow, the inflow and outflow boundary conditions are set for transonic flow upon eigen vectors characteristics.

For the upper and lower boundaries of the cascades, the periodic boundary condition was used to give the circumferential continuity of the cascade.

The physical domain was split to multi zones for using the multi-block technique and each block. Figure 2 shows the schematics shared area of the two adjacent blocks. The common walls of the rotor and stator rows shares their data in each time step as their adjacent wall boundary condition. However, the data exchanging from the relative frame to absolute frame was also added to the adjacent wall condition at the interface of the rotor and stator for the complete stage study.

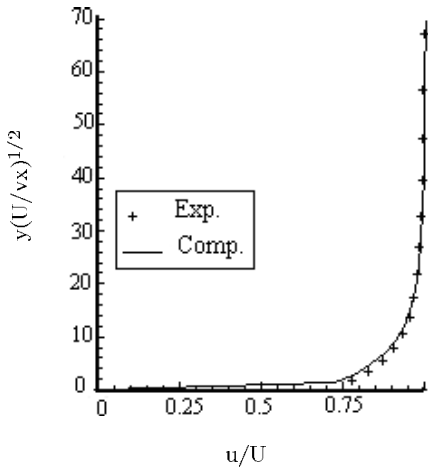

Figure 3. Comparing the computed velocity profile for flat plate with the experimental profile at 68% of plate length, from the leading edge of the flat plate.

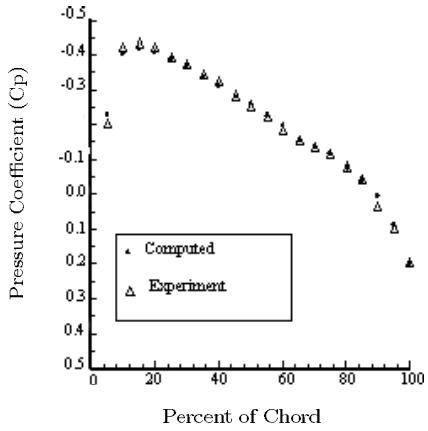

Figure 4. Computed and experimental Pressure coefficients over a semi NACA0012 airfoil. Mach number is 0.4 and Reynolds Number is 10^6.

Grid Generation

Each passage (between two blades) has an individual mesh, which is generated by mesh generator program using Partial Differential Equations (PDE) method. Clustering is available by related source terms as well as orthogonality. The mesh generated for each individual passage is considered as a single block, and the solver assembles them to prepare the complete area of solution by using the multi-block boundary condition. The resolution is chosen upon grid dependency studies, which show that a 75×41 grid for each block has a minimum CPU time without any grid dependency of the results.

Turbulence Modeling

An algebraic model, which is not written in terms of the boundary layer quantities and is very robust in separated regions, is the modified Baldwin-Lomax (BL) model ([9]). The BL model is implemented by He [6] in numerical investigation of Rotating-Stall inception in a multi-blade cascade flow in an axial compressor, in which the flow may have large scale separated zones. Moreover, the comparison of other turbulence models such as κ-ϵ with BL model, done by Bohn *et.al.* [11], shows adequate assurance using BL model in cascade problems. Although a large amount of memory is required in multi-blades studies, the BL requires the least amount of memory and CPU time with respect to higher-order turbulence models. Consequently, in the present work the BL model is preferred.

DISCUSSION OF RESULTS

Code Validations Studies

The performance of the described methodology is assessed by comparing the computed results with other verified data.

The first test case is performed on flow over a flat plate in incompressible range of the Mach number ($M = 0.2$). The Reynolds number is 10^6, and the

transition point is set at leading edge of the plate. This study gives adequate assurance of viscous solution of the solver with the implemented turbulence model.

Additionally, the good agreement of the results with those reported by Bohn *et.al.* shown in Figure 3 shows that the grid resolution 200×80 used for the computational domain is sufficient to capture the boundary layer.

The second test study is performed on the subsonic viscous flow over a NACA0012 airfoil. The Reynolds number is set to 10^6 and the flow is turbulent. The inlet Mach number is set to 0.4, and the angle of attack is set to zero. Figure 4, shows the computed results, which are in good agreement with experimental results reported by Fletcher [12].

The third test study is performed on the transonic viscous flow over a NACA0012 airfoil. The Reynolds number is set to 10^6 and the flow is turbulent. The inlet Mach number is set to 0.82 and the angle of attack is 2°. Figure 5 shows the computed results, which are in good agreement with the experimental results reported by Hirsch [13].

The final test is performed to evaluate the optimum grid. A two-passage stage which is a multi block system similar to that used for compressor stage simulation is chosen for the grid dependency study (Figure 6). Three grids are performed for the study and the grid 75× 41 (for each block) (Figure 7) seems to be adequate for the present study.

FLOW THROUGH A ROTOR OF AXIAL COMPRESSOR

The final studies are performed on the flow through a single rotor-cascade and the flow through a complete

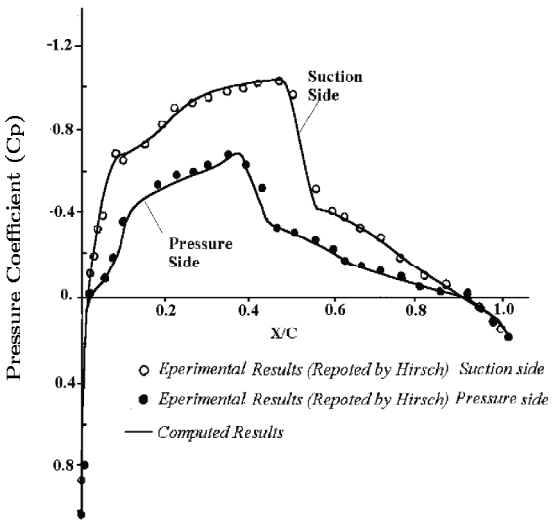

Figure 5. Computed and experimental Pressure coefficients over a semi NACA0012 airfoil. Mach number is 0.82, the Reynolds Number is 10^6, and at 2° angle of attack.

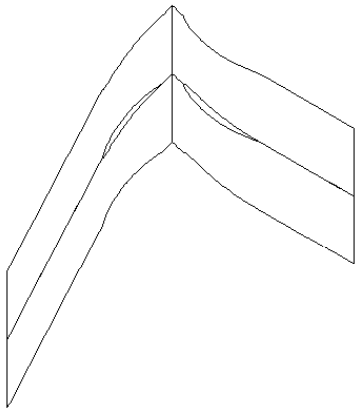

Figure 6. The geometry of the double passage stage used for the mesh dependency study.

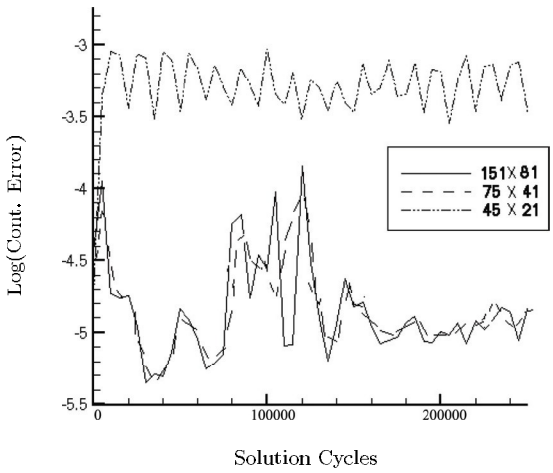

Figure 7. The Mesh dependency study upon convergence history.

2-D stage at the unstable operation point of an axial compressor.

The geometrical characteristics of the blades used in the cascades (rotor and stator rows) are given in Table 1, and the flow characteristics in the stable and unstable operating conditions are given in tables 2^{nd}, 3^{rd}, respectively. The thermodynamic path for choosing the unstable operating point near the stability limit line is shown in Figure 8.

The studies for the free-rotor and the complete stage cases were prepared for a set of cascade lengths

Table 1. Geometrical characteristics of the cascade.

Stagger angel of rotor blades	55
Stagger angel of stator blades	35
Rotor blade profile	NACA65-(A_{10})
Stator blade profile	NACA65-(A_{10})
Solidity	1.35

with 2, 4, 7, 9, 10, 11, 12, 14, and 16 blades. The blades are numbered from bottom to top. Near the leading edge of the odd blades in rotor row, numerical probes are located to indicate the axial velocity traces. To provide a clear imagination about the computational area, Figure 9 illustrates the 14-blade cascade for the free-rotor case and the complete stage case as a sample of all studied cases. The solid lines show the boundaries of each block (regarding the multi-block technique), and 7 probes are located near the leading edge of the blades.

The total number of finite volume cells is equal to: Number of blades 2×75×41. Figure 10 shows an enlarged section of the computational area for the free-rotor case to give a visual presentation of the used mesh.

The velocity traces for RS condition of the 14-blade and the 16-blade were nearly the same and they were sketched against the dimensionless time (rotor revolutions) and presented in Figure 11 for both geometric cases. For clarity, the time traces from each probe shown in Figure 11 are shifted by a constant interval, and the time is computed from the time of imposing the unstable conditions. It is noticed that this calculated RS pattern seems to be different from that commonly observed in experiments, where a single RS cell almost always comes into existence during a stall inception process. From the modal-wave point of view, the single-cell pattern should be associated with the first-order modal wave with its wave-length being the circumference. In the present case, no indication of the first-order modal-wave was observed. As He [6] studied,

Table 2. The stable condition.

r_h/r_t	0.6
R	0.56
P_{in}	100000 Pa
T_{in}	300 K°
$P_{exit}/\ P_{in}$	1.02589
β_1	62°
ψ	0.28
ϕ	0.4
V_{xin}	36 m/s
M_{in}	0.223
U_r	90 m/s
RPM	1240

Table 3. The unstable condition.

P_{exit}/P_{in}	1.02989
β_1	72°
V_{xin}	22 m/s
ϕ	0.24
RPM	1240

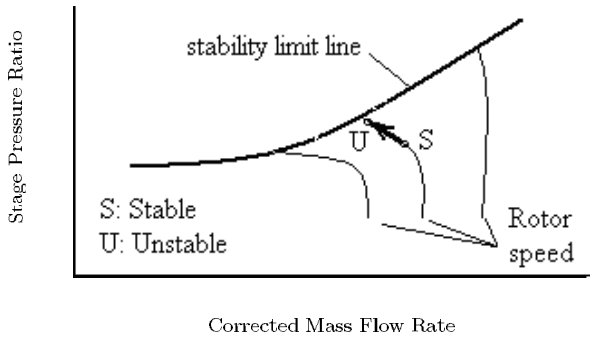

Figure 8. The thermodynamic path for reaching RS condition from the normal operating point.

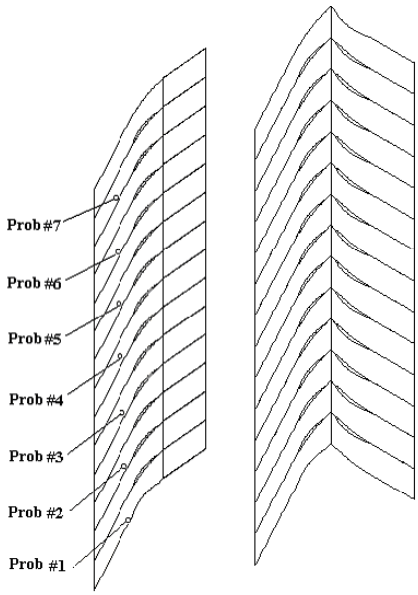

Figure 9. The 14-blade geometry and the probe location.

the reason is that the background noise in calculations was not big enough to trigger the first modal wave to grow.

The streamlines of 14-blade studies at the time of 2.83 of the rotor revolutions were shown in Figure 12. The deep cells happened approximately at every

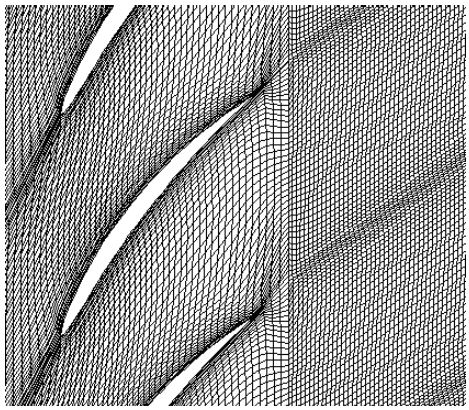

Figure 10. The sample enlarged mesh generated for rotor-cascade studies.

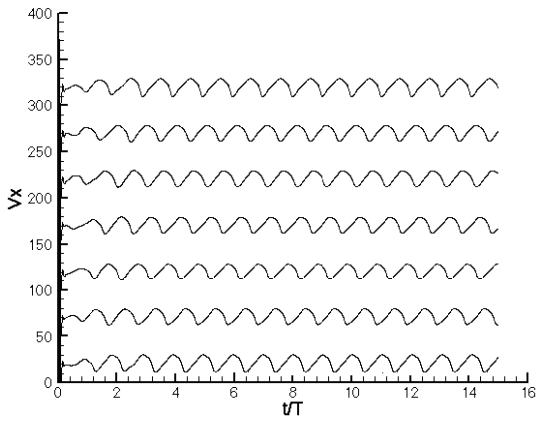

(a) Free-Rotor Cascade

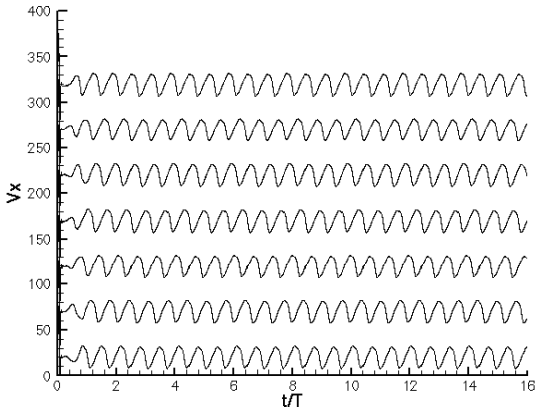

(b) The Complete Stage

Figure 11. Velocity traces for 14-Blades geometry. The traces are shifted with constant interval for clarity.

five blades distance from each other in both cases, and the streamlines seem to be nearly similar. Observing the velocity traces of the 14-blades cases shows that the deep cell frequencies of the two cases are nearly the same but the amplitudes are obviously different. The results of r the 16-blade show similar behaviors for the streamlines and the velocity traces and, therefore, are not repeated here. The velocity traces for the 12, 11, 9, 7, and 4 blades are shown in Figures 11 to 17 respectively. The comparison of the velocity between the free-rotor and the complete stage approaches in each number of blades shows that the differences in frequencies and the amplitudes of the velocity traces are not negligible. This means that the modal shapes of RS for the two geometric approaches differ from each other when the number of blades decreases. However, this also shows that decreasing the number of blades below a minimum value may affect the modal shapes of RS, and any chosen number of blade can probably trigger one of the modal shapes of RS. Reconsidering the velocity traces for various numbers of blades concludes 2 or three modal shapes for the RS. The modes of 4, 9 and 14 blades-cascades (mode A) are nearly

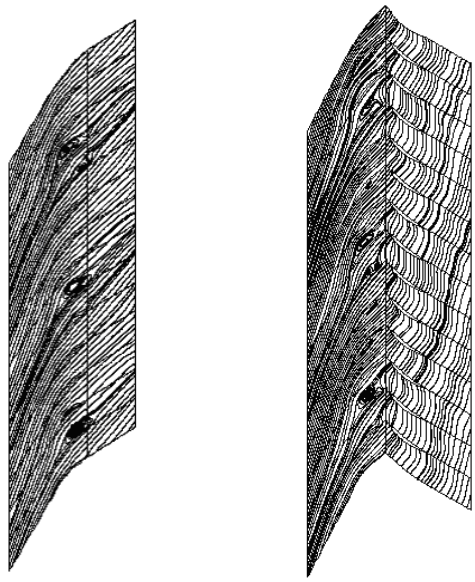

(a) Free-Rotor (b) The Complete Stage

Figure 12. The unstable streamlines for 14 and 16 blades geometry at time 2.83 rotor revolutions.

the same in frequency and amplitude, but they differ in stall initiation. Similarly, the modal shapes of RS for the 7 and 12 blades cases (mode B) are nearly the same, but the modes A and B are obviously different in modal characteristics. The results of 11 blades of the free-rotor case magnify the existence of a third mode for RS, but this does not render the same result for the complete stage problem. Figure 18 provides a brief comparison of modal characteristics of the deep cells during the RS effect. It illustrates the frequency variation against the number of blades for the stage with and without stator cascade. The results show that in values lower than 14 for the number of blades blades, the frequency of the velocity traces (deep cell repeating frequency) varies apparently for the complete and semi stages. Figure 18 also shows that after 14 blades, the frequencies of the two geometric approaches are nearly the same, but the frequency varies when the number of blades increases from a minimum value. Similar results are achieved when considering Figure 19, where the duration time of a complete growth of a deep cell in RS (stall initiation) is sketched against the number of blades for the complete and semi stages. The results of Figure 19 again show that after about 14, there is no dependency between the stall initiation and the number of blades for both geometric approaches. This realty validates the forced noise method used by He [6] for observing a wide range of RS modal shapes.

CONCLUDING REMARKS

A multi-block 2-D solver was employed to investigate the viscous through-flow in stage of axial compressor. Three test cases gave provided assurance for

employment of the code. The rotating stall effect was numerically observed for the flow through a complete (with stator) and a semi-stage axial compressor. The RS was studied for both cases in a relatively wide range of cascade lengths. The following conclusions are noteworthy:

1. All velocity traces show a periodic behavior similar

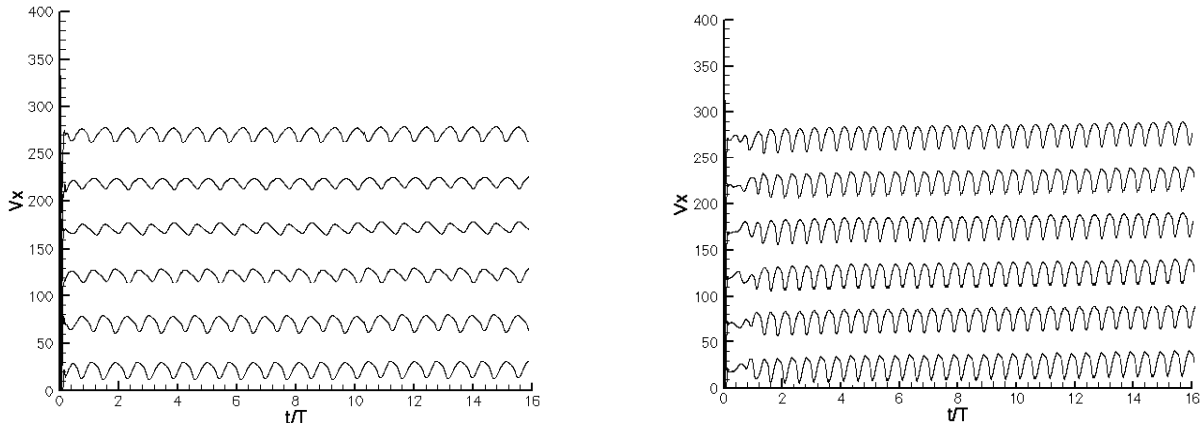

(a) Free-Rotor (b) The Complete Stage

Figure 13. Velocity traces for 12-Blade geometry during the RS effect. The traces are shifted with constant intervals for clarity.

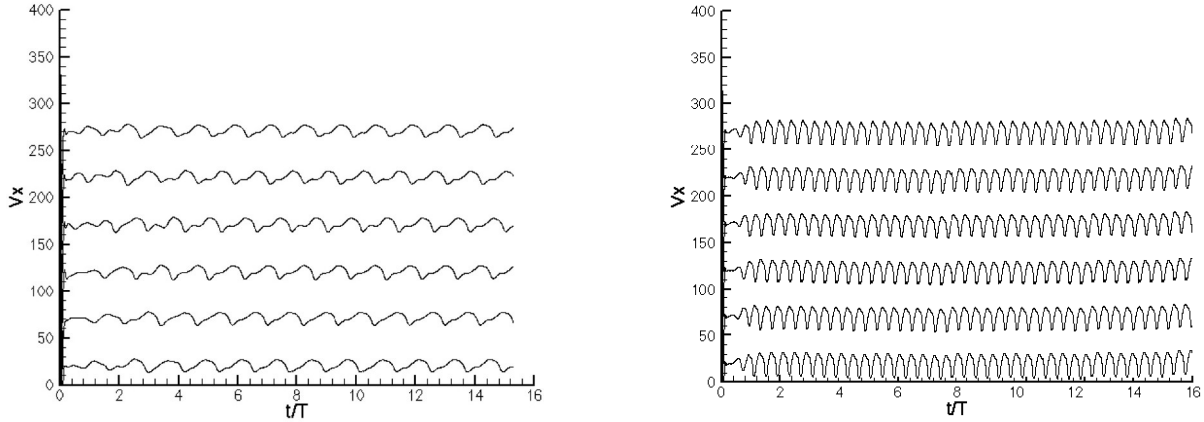

(a) Free-Rotor (b) The Complete Stage

Figure 14. Velocity traces for 11-Blades geometry during the RS effect. The traces are shifted with constant intervals for clarity.

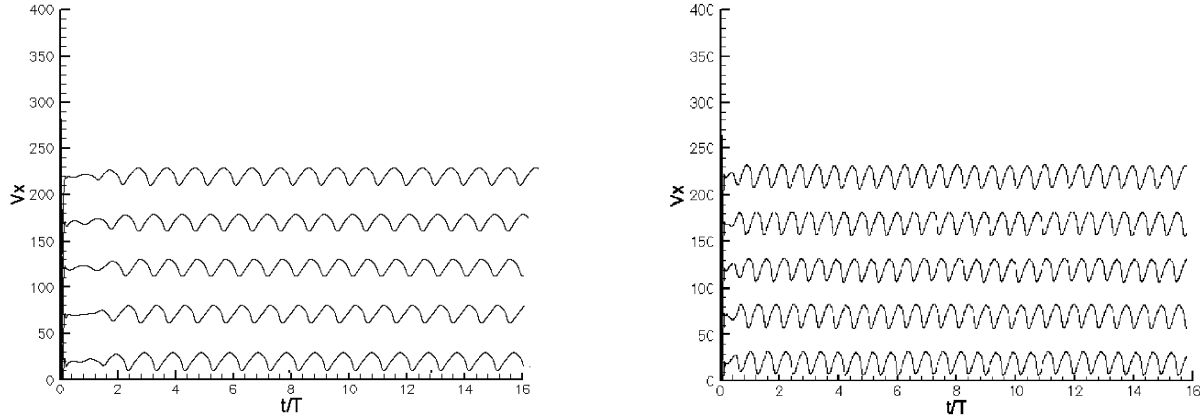

(a) Free-Rotor (b) The Complete Stage

Figure 15. Velocity traces for 9-Blade geometry during the RS effect. The traces are shifted with constant intervals for clarity.

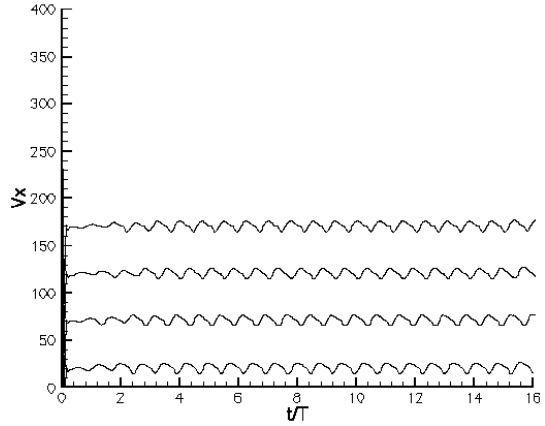

(a) Free-Rotor

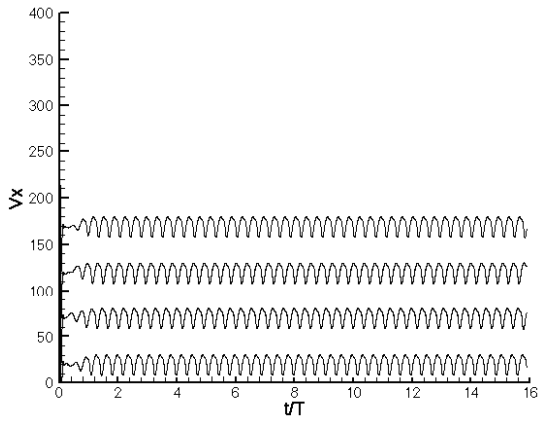

(b) The Complete Stage

Figure 16. Velocity traces for 7-Blades geometry during the RS effect. The traces are shifted with constant intervals for clarity.

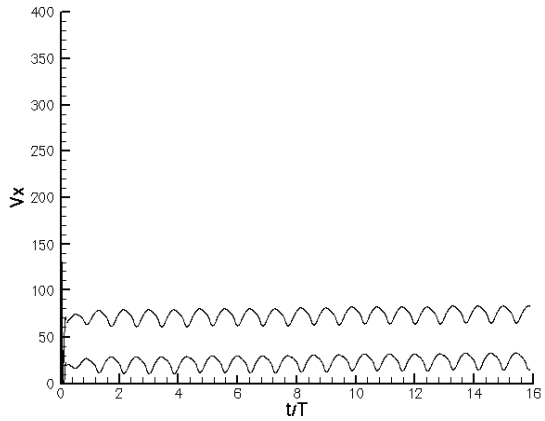

(a) Free-Rotor

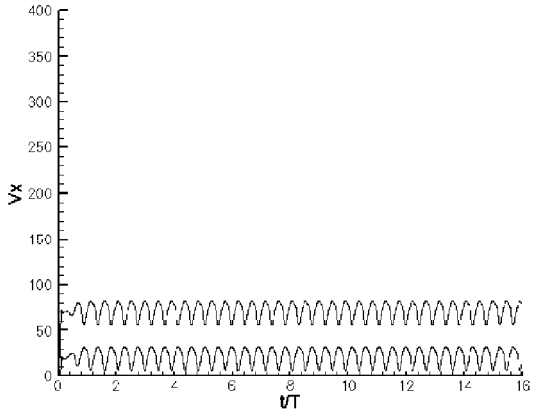

(b) The Complete Stage

Figure 17. Velocity traces for 4-Blades geometry during the RS effect. The traces are shifted with constant intervals for clarity.

to previous reports (He [6] and Saxer [8]), for any chosen number of blades in RS phenomena for both main approaches.

2. Comparing velocity traces shows that there are approximately at least two major modes for RS during the variation of cascade length lower than 14 blades, and the modal shapes of RS do not vary after 14 blades. The cascade length does not affect the captured modal characteristics of the RS. This may be related to that distance of the periodic boundary conditions of the lower and upper boundaries in longer cascades is for enough.
3. Both geometric approaches of the complete and the semi stages nearly show the same behavior of RS deep cells during the variation of cascade length, but the frequency and stall initiation times vary in different levels for the two cases.
4. Even though using lower cascade lengths apparently causes different modes of RS, the modes seem to be artificial results of boundary effects and unstable behavior of the flow. As a result, the employment of higher numbers of blades in modal studies of the RS needs an exciting noise to trigger different real modal shapes of the RS. This conclusion validates using forced pressure noise method in modal studies of RS used by He [6].
5. In RS modal studies, the employment of semi-stage approach causes errors in frequency of RS, and its propagation speed. Consequently the complete stage seems to be a better approach.
6. All cases show that without any consideration of modal characteristic studies of the RS even the 4 blades case, with free-rotor approach (the much simpler geometry), can predict the instability, which is a useful help to minimize the CPU times and the required memories in CFD investigations during the off-design prediction studies of the axial compressors. The off-design prediction determines

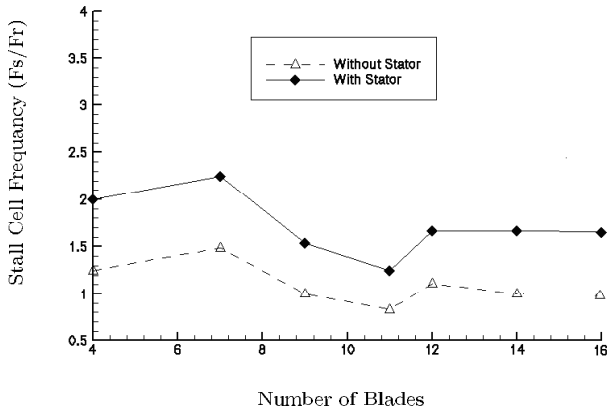

Figure 18. Variation of the frequency of the vortex oscillation in circumferential direction at the RS effect for the stage with and without stator cascades.

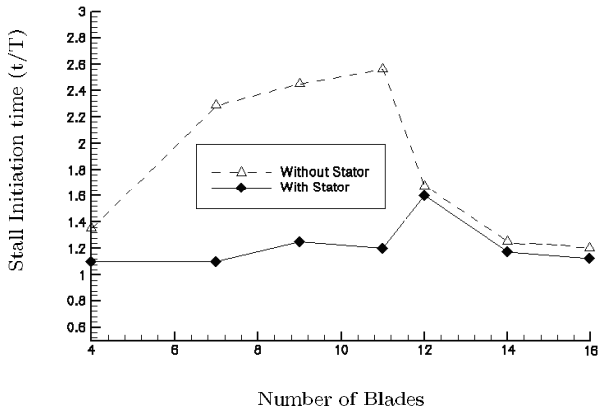

Figure 19. Variation of the RS initiation time against the variation of the cascade length for the stage with and without stator cascades.

the location of the stability limit line in compressor maps.

REFERENCES

1. Inue, M., Kuroumaru, M., Tanino, T., and Furukawa, M., "Propagation of Multiple Short-Length-Scale Stall Cells in an Axial Compressor Rotor", *ASME J. of Turb.*, **122**, PP 45-53(2000).
2. Day, I. J., Breuer, T., Escuret, J., Cherrett, M., and Wilson, A., "Stall Inception and the Prospects for Active Control in Four High-Speed Compressors", *ASME J. of Turb.*, **121**, PP 18-27(1999).
3. Silowski, P. D., "Measurements of Rotor Stalling in a Matched and a Mismatched Multistage Compressor", *GTL Report*, Gas Turbine Laboratory, Massachusetts Institute of Technology, **221**, (1995).
4. Sisto, F., Wu, W., Thangam, S., and Jonnavithula, S., "Computational Aerodynamics of Oscillating Cascade with Evolution of Rotating Stall", *AIAA Journal*, **27**, PP 462-471(1989).
5. Jonnavithula, S., Thangam, S., and Sisto, F., "Computational and Experimental Study of Stall Propagation in Axial Compressors", *AIAA Journal* , **28**, PP 1945-1952(1990).
6. He L., "Computational Study of Rotating-Stall Inception in Axial Compressors", *Journal of Propulsion and Power*, **13**, PP 31-38(1997).
7. Outa, E., Kato, D., and Chiba, K., "A N-S Simulation of Stall Cell Behavior in a 2-D Compressor Rotor-Stator System at Various Load", *ASME Paper 94-GT-257*, (1994).
8. Saxer-Flelici, H. M., Saxer, A. P., Inderbitzen, A., Gyarmathy, G., "Prediction and Measurement of Rotating Stall Cell in an Axial Compressor", *ASME Journal of Turbomachinery*, **121**, PP 365-375(1999).
9. Hoffman, K. A., Chiang, S. T., *Computational Fluid Dynamics for Engineers*, A Publication of Engineering Education SystemTM, (1993).
10. Peyret, R., Grasso, F., and Meola, C., *Handbook of Computational Fluid Mechanics*, Academic Press, (1996).
11. Bohn D. and Emunds R., "A Navier-Stokes Computer Code for Theoretical Investigations on the Application of Various Turbulence Models for Flow Prediction Along Turbine Blades", *Proceeding of the International Gas Turbine and Aero-engine Congress and Exposition*, Houston, Texas, (1995).
12. Fletcher, C. A. J., *Computational Techniques for Fluid Dynamics 2*, (1991).
13. Hirsch, C., *Numerical Computation of Internal and External Flows*, A wiley-Interscience Publication, (1988).